

Received March 23, 2020, accepted April 5, 2020, date of publication April 8, 2020, date of current version April 24, 2020.

Digital Object Identifier 10.1109/ACCESS.2020.2986715

# Adaptive UT- $H_\infty$ Filter for SINS' Transfer Alignment Under Uncertain Disturbances

WEIWEI LYU<sup>1,2</sup>, XIANGHONG CHENG<sup>1,2</sup>, AND JINLING WANG<sup>1,3</sup>

<sup>1</sup>School of Instrument Science and Engineering, Southeast University, Nanjing 210096, China

<sup>2</sup>Key Laboratory of Micro-Inertial Instrument and Advanced Navigation Technology of Ministry of Education, Southeast University, Nanjing 210096, China

<sup>3</sup>School of Civil and Environmental Engineering, University of New South Wales, Sydney, NSW 2052, Australia

Corresponding author: Xianghong Cheng (xhcheng@seu.edu.cn)

This work was supported in part by the National Natural Science Foundation of China under Grant 61773116, in part by the Fundamental Research Funds for the Central Universities, in part by the Postgraduate Research and Practice Innovation Program of Jiangsu Province under Grant KYCX17\_0103, in part by the Scientific Research Foundation of Graduate School of Southeast University under Grant YBJJ1847, and in part by the Shanghai Aerospace Science and Technology Innovation Fund under Grant SAST2019079.

**ABSTRACT** Accurate and rapid transfer alignment with large attitude errors under uncertain disturbances is crucial for the strapdown inertial navigation system (SINS). This paper proposes an adaptive UT- $H_\infty$  filter which combines UKF technology and a  $H_\infty$  filter to increase the robustness of the nonlinear transfer alignment system. By focusing on the time-varying and the uncertain external disturbances, the robustness factor of the adaptive UT- $H_\infty$  filter can be adaptively adjusted to balance the robustness and filtering accuracy of the dynamic system. Then, the nonlinear error propagation model of the transfer alignment is established in detail, and the velocity plus attitude matrix measurement model is used to improve the performance of transfer alignment. Moreover, the sensor error compensation model is established to calibrate and compensate for the sensor errors of the gyros and accelerometers online during transfer alignment. The vehicle transfer alignment experiments show that the proposed adaptive UT- $H_\infty$  filter can significantly improve the transfer alignment accuracy and the pure inertial navigation accuracy compared with the existing filtering methods under uncertain disturbances.


**INDEX TERMS** Transfer alignment; nonlinear error model; adaptive UT- $H_\infty$  filter; robustness; uncertain disturbances.

## I. INTRODUCTION

A strapdown inertial navigation system (SINS) is an all-weather independent navigation system which can provide accurate three-dimensional information on attitude, velocity and position of a vehicle [1], [2]. As the performance of the SINS is greatly influenced by the accuracy and rapidness of the initial alignment [3]–[5], it is crucial to study the initial alignment methods when the SINS is used in different application scenarios. In general, the initial alignment can be classified into self-alignment, transfer alignment, and combination alignment [6]. Compared with the other two alignment modes, transfer alignment has two significant advantages. One is that transfer alignment is more rapid, so it can be completed in a shorter time [7]. The other is that self-alignment and combination alignment require high sensor accuracy [3], [4], [6]; when the SINS has low sensor

accuracy, the initial alignment cannot be completed by the two alignment modes. However, there is no such problem for transfer alignment, and transfer alignment also applies to a low accuracy SINS [2]. Based on the above advantages, transfer alignment has a wide range of applications such as aircrafts, ships and vehicles [5], [8].

The error propagation model and filtering algorithm are two important aspects of the transfer alignment of the SINS [9]. The error sources of the SINS include inertial measurement errors, initial condition errors, external disturbances, environmental model errors and others [1], [7]. The error propagation model of SINS is described by a group of nonlinear differential equations [9], [10]. The classical linear error model of the small misalignment angle can only be established under the assumption that the error sources are small. However, with the rapid development of SINS technology, the application of the classical linear error model is limited, and it is necessary to study the nonlinear error propagation model and the nonlinear

The associate editor coordinating the review of this manuscript and approving it for publication was Halil Ersin Soken .

filtering algorithm [10]–[12]. According to the premise of priori course uncertainty, Dmitriyev *et al.* [9] derived nonlinear equations which describe the behavior of inertial navigation system (INS) errors in the initial alignment. In [5], to solve the problem of strong nonlinearity of the transfer alignment model on vertically launched and warship-borne missiles, a central difference particle filter (CDPF) was proposed. The above studies have established accurate nonlinear error propagation models of transfer alignment, and nonlinear filtering algorithms have been used. However, there are actually a lot of errors and disturbances between the master SINS (M-SINS) and the slave SINS (S-SINS) in practical applications. They include flexure deformation, lever arm effect, installation errors, vibration of vehicle, unknown environmental disturbances, and so on. And many of the errors and disturbances are time-varying and change with the application environment, which are difficult to be modeled accurately. When the nonlinear error model cannot be accurately established [13]–[15], or the external disturbances are uncertain and time-varying [16]–[19], how to complete accurate and rapid transfer alignment is a challenging problem to be solved.

For the nonlinear filtering problem, the common approaches are based on an extended Kalman filter (EKF) or an unscented Kalman filter (UKF) [20]–[22]. EKF uses first-order linearization of the nonlinear function, so it is only used for the weak nonlinear model [21]. UKF uses the distribution of sigma points to approximately represent the distribution of the nonlinear function, and the estimation accuracy can achieve at least second order [20], [23]. To use the third-degree spherical-radial cubature rule, Arasaratnam *et al.* [24] designed the cubature Kalman filter (CKF) for the high-dimensional state estimation. It can be proven that CKF is actually a special case of UKF when the tune parameter  $\kappa$  of UKF is set to zero [23]. However, EKF, UKF and CKF all require the accurate nonlinear error model and the exact noise statistics, which are very hard to be satisfied in real-world systems [16]. The incomplete information of the dynamical system and the uncertain and time-varying external disturbances can lead to the decrease of the estimation accuracy or even filtering divergence [16], [18], [25]–[27]. Therefore, it is necessary to study new robust filtering algorithms to improve the filtering performance for practical applications [18], [25], [28]–[30]. Jia *et al.* [17] designed a Sparse-grid Quadrature Filter (SGQF) which utilizes weighted sparse-grid quadrature points to approximate the multidimensional integrals, and the estimation accuracy level of the SGQF can be flexibly controlled. Based on an approximation to the quadratic error matrix, Hu *et al.* [31] derived a second-order extended (SOE) H $\infty$  filter for nonlinear discrete-time systems that have model uncertainty. In [32], an adaptive event-triggered H $\infty$  filter was designed for a class of networked nonlinear interconnected systems. These studies have intensively explored robust filtering, but few studies have been done for the nonlinear error model of transfer alignment.

In this paper, a novel adaptive UT-H $\infty$  filter is designed for SINS' transfer alignment under uncertain disturbances. Different from the linear transfer alignment method in [7], this paper aims to solve the nonlinear transfer alignment problem, and a nonlinear filtering method for transfer alignment is proposed. The adaptive UT-H $\infty$  filter combines the UKF technology and H $\infty$  filter to increase the robustness of the nonlinear system. The robustness factor  $\xi$  of the adaptive UT-H $\infty$  filter is dynamically adjusted when the external environment changes. Then, a nonlinear transfer alignment model is established, which includes the SINS nonlinear error model, velocity plus attitude matrix measurement model and the sensor error compensation model. The vehicle transfer alignment experiments verify the better robustness and higher estimation accuracy of the proposed adaptive UT-H $\infty$  filter under uncertain disturbances.

The structure of this paper is as follows. In Section II, UKF filtering technology is described. In Section III, the recursive algorithm of UT-H $\infty$  filter is derived rigorously, and the adaptive UT-H $\infty$  filter is designed. The nonlinear transfer alignment model is established in detail in Section IV. In Section V, twenty groups of vehicle transfer alignment field experiments are performed to verify the effectiveness of the proposed method. Finally, conclusions are given in Section VI.

## II. UKF TECHNOLOGY

Consider the following nonlinear discrete-time system with additive noise [12], [31]:

$$\begin{aligned} \mathbf{X}_{k+1} &= f(\mathbf{X}_k) + \mathbf{\Gamma}_k \mathbf{W}_k \\ \mathbf{Y}_k &= \mathbf{H}_k \mathbf{X}_k + \mathbf{V}_k \end{aligned} \quad (1)$$

where  $\mathbf{X}_k$  is the  $(N \times 1)$  state estimate;  $f(\cdot)$  is a nonlinear function;  $\mathbf{\Gamma}_k$  is the  $(N \times T)$  system noise matrix;  $\mathbf{Y}_k$  is the  $(M \times 1)$  measurement value;  $\mathbf{H}_k$  is the  $(M \times N)$  measurement matrix;  $\mathbf{W}_k$  is the  $(T \times T)$  system process noise matrix; and  $\mathbf{V}_k$  is the measurement noise matrix. Here,  $\mathbf{W}_k$  and  $\mathbf{V}_k$  are the uncorrelated zero-mean Gaussian white sequences, and they satisfy the following relationships [22]:

$$\begin{aligned} E[\mathbf{W}_j \mathbf{W}_k^T] &= \delta_{jk} \mathbf{Q}_k \\ E[\mathbf{V}_j \mathbf{V}_k^T] &= \delta_{jk} \mathbf{R}_k \\ E[\mathbf{W}_j \mathbf{V}_k^T] &= 0 \end{aligned} \quad (2)$$

In the above equation,  $\mathbf{Q}_{k \geq 0}$ , and  $\mathbf{R}_{k > 0, \delta_{jk}}$  is the Kronecker function, i.e.,

$$\delta_{jk} = \begin{cases} 0 & (k \neq j) \\ 1 & (k = j). \end{cases}$$

The implementation of the simplified UKF algorithm is presented as follows:

(1) Initialization:

$$\begin{aligned} \hat{\mathbf{X}}_0 &= E[\mathbf{X}_0] \\ \mathbf{P}_0 &= E\left[(\mathbf{X}_0 - \hat{\mathbf{X}}_0)(\mathbf{X}_0 - \hat{\mathbf{X}}_0)^T\right] \end{aligned} \quad (3)$$

(2) Time updating:

$$\begin{aligned} \mathbf{X}_0 &= \hat{\mathbf{X}}_{k-1} \\ \mathbf{X}_i &= [\hat{\mathbf{X}}_{k-1}]_N + \sqrt{(N + \gamma)\mathbf{P}_{k-1i}} \quad i = 1, 2, \dots, N \\ \mathbf{X}_i &= [\hat{\mathbf{X}}_{k-1}]_N - \sqrt{(N + \gamma)\mathbf{P}_{k-1i-N}} \\ & \quad i = N + 1, N + 2, \dots, 2N \end{aligned} \quad (4)$$

$$\mathbf{X}_{k|k-1} = f(\mathbf{X}_{k-1})$$

$$\begin{aligned} \hat{\mathbf{X}}_{k|k-1} &= \sum_{i=0}^{2N} W_i^m \mathbf{X}_{i,k|k-1} \\ \mathbf{P}_{xx,k|k-1} &= \sum_{i=0}^{2N} W_i^c \left( \mathbf{X}_{i,k|k-1} - \hat{\mathbf{X}}_{k|k-1} \right) \\ & \quad \times \left( \mathbf{X}_{i,k|k-1} - \hat{\mathbf{X}}_{k|k-1} \right)^T + \mathbf{\Gamma}_{k-1} \mathbf{Q}_{k-1} \mathbf{\Gamma}_{k-1}^T \end{aligned} \quad (5)$$

(3) Measurement updating:

$$\begin{aligned} \mathbf{K}_k &= \mathbf{P}_{xx,k|k-1} \mathbf{H}_k^T \left( \mathbf{H}_k \mathbf{P}_{xx,k|k-1} \mathbf{H}_k^T + \mathbf{R}_k \right)^{-1} \\ \hat{\mathbf{X}}_k &= \hat{\mathbf{X}}_{k|k-1} + \mathbf{K}_k \left( \mathbf{Z}_k - \hat{\mathbf{Z}}_{k|k-1} \right) \\ \mathbf{P}_k &= \left( \mathbf{I} - \mathbf{K}_k \mathbf{H}_k \right) \mathbf{P}_{xx,k|k-1} \end{aligned} \quad (6)$$

The parameters for calculating the sigma points are given as follows:

$$\begin{aligned} \gamma &= \alpha^2 (N + \kappa) - N \\ W_0^m &= \gamma / (N + \gamma) \\ W_0^c &= \gamma / (N + \gamma) + \left( 1 - \alpha^2 + \beta \right) \\ W_i^m &= W_i^c = 1/2 (N + \gamma) \quad i = 1, 2, \dots, 2N \end{aligned} \quad (7)$$

where  $W^m$  and  $W^c$  represent the mean weight and covariance weight, respectively;  $N$  is the dimension of the system state;  $\alpha$  is a small positive number and  $1e-4 \leq \alpha \leq 1$ ;  $\kappa = 3 - N$ ; the value of  $\beta$  is relative to the distribution of  $X$ , and for the normal distribution,  $\beta = 2$  is optimal [10].

### III. ADAPTIVE UT-H $\infty$ FILTER

#### A. UT-H $\infty$ FILTER

Considering the following nonlinear discrete-time system with additive noise:

$$\begin{aligned} \mathbf{X}_{k+1} &= f(\mathbf{X}_k) + \mathbf{\Gamma}_k \mathbf{W}_k \\ \mathbf{Y}_k &= \mathbf{H}_k \mathbf{X}_k + \mathbf{V}_k \end{aligned} \quad (8)$$

where  $\mathbf{\Gamma}_k$  is the  $(N \times T)$  system noise matrix;  $\mathbf{W}_k$  is the  $(T \times T)$  system process noise matrix; and  $\mathbf{V}_k$  is the measurement noise matrix. The difference between Equation (1) and Equation (8) is that  $\mathbf{\Gamma}_k$  is unknown, and we do not make assumptions about the statistical properties of  $\mathbf{W}_k$  and  $\mathbf{V}_k$  in Equation (8).

In general, some arbitrary linear combination of the system states needs to be estimated; that is,  $\mathbf{Z}_k = \mathbf{L}_k \mathbf{X}_k$ , where  $\mathbf{L}_k$  is a given  $(N \times N)$  matrix. Therefore, the system model in Krein

space can be obtained by extending  $\mathbf{Z}_k$  to the measurement value; it can be expressed as follows [26], [27]:

$$\begin{aligned} \mathbf{X}_{k+1} &= f(\mathbf{X}_k) + \mathbf{\Gamma}_k \mathbf{W}_k \\ \begin{bmatrix} \mathbf{Y}_k \\ \mathbf{Z}_k \end{bmatrix} &= \begin{bmatrix} \mathbf{H}_k \\ \mathbf{L}_k \end{bmatrix} \mathbf{X}_k + \mathbf{V}'_k \end{aligned} \quad (9)$$

where  $\mathbf{W}_k$  and  $\mathbf{V}'_k$  are the noise with bounded energy, and their statistical characteristics are not assumed to be Gaussian noise.  $\mathbf{X}_0$ ,  $\mathbf{W}_k$  and  $\mathbf{V}'_k$  satisfy the following relationship:

$$E \left[ \left\langle \begin{bmatrix} \mathbf{X}_0 \\ \mathbf{W}_j \\ \mathbf{V}'_j \end{bmatrix}, \begin{bmatrix} \mathbf{X}_0 \\ \mathbf{W}_k \\ \mathbf{V}'_k \end{bmatrix} \right\rangle \right] = \begin{bmatrix} \mathbf{P}_0 & \mathbf{0} & \mathbf{0} \\ \mathbf{0} & \mathbf{I} \delta_{jk} & \mathbf{0} \\ \mathbf{0} & \mathbf{0} & \begin{bmatrix} \mathbf{I} & \mathbf{0} \\ \mathbf{0} & -\xi^2 \mathbf{I} \end{bmatrix} \delta_{jk} \end{bmatrix} \quad (10)$$

where  $\xi$  is the robustness factor of the UT-H $\infty$  filter.

According to the simplified UKF algorithm, the sigma points and their propagation results need to be calculated, and they can be expressed as follows:

$$\begin{aligned} \mathbf{X}_0 &= \hat{\mathbf{X}}_{k-1} \\ \mathbf{X}_i &= [\hat{\mathbf{X}}_{k-1}]_N + \sqrt{(N + \gamma)\mathbf{P}_{k-1i}} \quad i = 1, 2, \dots, N \\ \mathbf{X}_i &= [\hat{\mathbf{X}}_{k-1}]_N - \sqrt{(N + \gamma)\mathbf{P}_{k-1i-N}} \\ & \quad i = N + 1, N + 2, \dots, 2N \end{aligned} \quad (11)$$

$$\mathbf{X}_{k|k-1} = f(\mathbf{X}_{k-1})$$

$$\begin{aligned} \hat{\mathbf{X}}_{k|k-1} &= \sum_{i=0}^{2N} W_i^m \mathbf{X}_{i,k|k-1} \\ \mathbf{P}_{xx,k|k-1} &= \sum_{i=0}^{2N} W_i^c \left( \mathbf{X}_{i,k|k-1} - \hat{\mathbf{X}}_{k|k-1} \right) \\ & \quad \times \left( \mathbf{X}_{i,k|k-1} - \hat{\mathbf{X}}_{k|k-1} \right)^T + \mathbf{\Gamma}_{k-1} \mathbf{\Gamma}_{k-1}^T \end{aligned} \quad (12)$$

Then, define the estimation error of the UT-H $\infty$  filter as:

$$\mathbf{e}_{f,k} = \hat{\mathbf{Z}}_k - \mathbf{L}_k \mathbf{X}_k \quad (13)$$

Define  $T_k(F_f)$  as the transfer function from the unknown disturbance  $\{(\mathbf{X}_0 - \hat{\mathbf{X}}_0), \mathbf{W}_k, \mathbf{V}_k\}$  in the  $h_2$  norm to the filtering error  $\{\mathbf{e}_k\}$ . When giving a positive number  $\xi$  ( $\xi > 0$ ), the goal of the UT-H $\infty$  filter is to search for suboptimal H $\infty$  estimation to satisfy the following relationship [26], [31]:

$$\begin{aligned} & \inf_{F_f} \|T_k(F_f)\|_{\infty}^2 \\ &= \inf_{F_f} \sup_{\mathbf{X}_0, \mathbf{W} \in h_2, \mathbf{V} \in h_2} \\ & \quad \times \frac{\|\mathbf{e}_{f,k}\|_2^2}{\|\mathbf{X}_0 - \hat{\mathbf{X}}_0\|_{\mathbf{P}_0^{-1}}^2 + \|\mathbf{W}_k\|_2^2 + \|\mathbf{V}'_k\|_2^2} \leq \xi^2 \end{aligned} \quad (14)$$

where the notation  $\|A\|_{\mathbf{W}}^2$  is defined as the square of the weighted  $h_2$  norm of  $A$ , i.e.,  $\|A\|_{\mathbf{W}}^2 = A^T \mathbf{W} A$ . The matrix  $\mathbf{P}_0$  is a positive definite matrix.

Based on Equation (14), the following theorem can be given [26]:

*Theorem 1 (Suboptimal H $\infty$  Filter Problem):* When given a positive number  $\xi > 0$ , if  $[\Phi_{k,k-1} \ \mathbf{G}_{k,k-1}]$  is full rank, then the condition that there is a filter satisfying  $\|\mathbf{T}_k(\mathbf{F}_f)\|_\infty < \xi$  if and only if

$$\mathbf{P}_k^{-1} + \mathbf{H}_k^T \mathbf{H}_k - \xi^{-2} \mathbf{L}_k^T \mathbf{L}_k > 0 \quad (15)$$

where  $\Phi_{k,k-1}$  is the  $(N \times N)$  state transition matrix.

To apply the recursive Riccati equation of the H $\infty$  filter in the linear system to the UT-H $\infty$  filter in the nonlinear system, the recursive Riccati equation needs to be transformed. Because  $\mathbf{P}_k|_{k-1}$  in the linear system can be obtained by  $\mathbf{P}_{xx,k}|_{k-1}$  after UT transformation in the nonlinear system, the recursive Riccati equation of the UT-H $\infty$  filter can be represented as follows:

$$\mathbf{P}_k = \left( \mathbf{I} - \mathbf{P}_{xx,k}|_{k-1} \begin{bmatrix} \mathbf{H}_k^T & \mathbf{L}_k^T \end{bmatrix} \mathbf{R}_{e,k}^{-1} \begin{bmatrix} \mathbf{H}_k \\ \mathbf{L}_k \end{bmatrix} \right) \mathbf{P}_{xx,k}|_{k-1} \quad (16)$$

where

$$\mathbf{R}_{e,k} = \begin{bmatrix} \mathbf{I} & 0 \\ 0 & -\xi^2 \mathbf{I} \end{bmatrix} + \begin{bmatrix} \mathbf{H}_k \\ \mathbf{L}_k \end{bmatrix} \mathbf{P}_{xx,k}|_{k-1} \begin{bmatrix} \mathbf{H}_k^T & \mathbf{L}_k^T \end{bmatrix}.$$

Therefore, the recursion of  $\hat{\mathbf{X}}_k$  is as follows:

$$\hat{\mathbf{X}}_k = \hat{\mathbf{X}}_{k|k-1} + \mathbf{K}_k \left( \mathbf{Y}_k - \mathbf{H}_k \hat{\mathbf{X}}_{k|k-1} \right) \quad (17)$$

where

$$\mathbf{K}_k = \mathbf{P}_{xx,k}|_{k-1} \mathbf{H}_k^T \left( \mathbf{H}_k \mathbf{P}_{xx,k}|_{k-1} \mathbf{H}_k^T + \mathbf{I} \right)^{-1} \quad (18)$$

Equation (16) needs to be simplified. By defining  $\mathbf{S}_{\infty,k} = \mathbf{P}_{xx,k}|_{k-1} \begin{bmatrix} \mathbf{H}_k^T & \mathbf{L}_k^T \end{bmatrix} \mathbf{R}_{e,k}^{-1}$ , Equation (16) can be rewritten as:

$$\mathbf{P}_k = \left( \mathbf{I} - \mathbf{S}_{\infty,k} \begin{bmatrix} \mathbf{H}_k \\ \mathbf{L}_k \end{bmatrix} \right) \mathbf{P}_{xx,k}|_{k-1} \quad (19)$$

$\mathbf{S}_{\infty,k}$  can be rearranged as:

$$\mathbf{S}_{\infty,k} = \begin{bmatrix} \mathbf{P}_{xx,k}|_{k-1} \mathbf{H}_k^T & \mathbf{P}_{xx,k}|_{k-1} \mathbf{L}_k^T \\ \times \left[ \begin{array}{cc} \mathbf{I} + \mathbf{H}_k \mathbf{P}_{xx,k}|_{k-1} \mathbf{H}_k^T & \mathbf{H}_k \mathbf{P}_{xx,k}|_{k-1} \mathbf{L}_k^T \\ \mathbf{L}_k \mathbf{P}_{xx,k}|_{k-1} \mathbf{H}_k^T & -\xi^2 \mathbf{I} + \mathbf{L}_k \mathbf{P}_{xx,k}|_{k-1} \mathbf{L}_k^T \end{array} \right]^{-1} \end{bmatrix} \quad (20)$$

Based on the inverse theorem of the partitioned matrix, we define:

$$\begin{aligned} \boldsymbol{\mu}_{11} &= \mathbf{I} + \mathbf{H}_k \mathbf{P}_{xx,k}|_{k-1} \mathbf{H}_k^T \\ \boldsymbol{\mu}_{12} &= \mathbf{H}_k \mathbf{P}_{xx,k}|_{k-1} \mathbf{L}_k^T \\ \boldsymbol{\mu}_{21} &= \mathbf{L}_k \mathbf{P}_{xx,k}|_{k-1} \mathbf{H}_k^T \\ \boldsymbol{\mu}_{22} &= -\xi^2 \mathbf{I} + \mathbf{L}_k \mathbf{P}_{xx,k}|_{k-1} \mathbf{L}_k^T \end{aligned} \quad (21)$$

Let:

$$\boldsymbol{\mu}^{-1} = \begin{bmatrix} \boldsymbol{\varphi}_{11} & \boldsymbol{\varphi}_{12} \\ \boldsymbol{\varphi}_{21} & \boldsymbol{\varphi}_{22} \end{bmatrix} \quad (22)$$

where  $\boldsymbol{\varphi}_{22} = (\boldsymbol{\mu}_{22} - \boldsymbol{\mu}_{21} \boldsymbol{\mu}_{11}^{-1} \boldsymbol{\mu}_{12})^{-1}$ ,  $\boldsymbol{\varphi}_{12} = -\boldsymbol{\mu}_{11}^{-1} \boldsymbol{\mu}_{12} \boldsymbol{\varphi}_{22}$ ,  $\boldsymbol{\varphi}_{21} = -\boldsymbol{\varphi}_{22} \boldsymbol{\mu}_{21} \boldsymbol{\mu}_{11}^{-1}$ ,  $\boldsymbol{\varphi}_{11} = \boldsymbol{\mu}_{11}^{-1} - \boldsymbol{\varphi}_{12} \boldsymbol{\mu}_{21} \boldsymbol{\mu}_{11}^{-1}$ .

Then:

$$\begin{aligned} \mathbf{S}_{\infty,k} &= \begin{bmatrix} \mathbf{P}_{xx,k}|_{k-1} \mathbf{H}_k^T & \mathbf{P}_{xx,k}|_{k-1} \mathbf{L}_k^T \end{bmatrix} \begin{bmatrix} \boldsymbol{\varphi}_{11} & \boldsymbol{\varphi}_{12} \\ \boldsymbol{\varphi}_{21} & \boldsymbol{\varphi}_{22} \end{bmatrix} \\ &= \begin{bmatrix} \mathbf{P}_{xx,k}|_{k-1} \mathbf{H}_k^T \boldsymbol{\varphi}_{11} + \mathbf{P}_{xx,k}|_{k-1} \mathbf{L}_k^T \boldsymbol{\varphi}_{21} \\ \mathbf{P}_{xx,k}|_{k-1} \mathbf{H}_k^T \boldsymbol{\varphi}_{12} + \mathbf{P}_{xx,k}|_{k-1} \mathbf{L}_k^T \boldsymbol{\varphi}_{22} \end{bmatrix} \end{aligned} \quad (23)$$

By defining  $\mathbf{S}_{\infty,k} = [\mathbf{S}_M \ \mathbf{S}_N]$ , firstly,  $\mathbf{S}_M$  can be simplified as:

$$\begin{aligned} \mathbf{S}_M &= \mathbf{P}_{xx,k}|_{k-1} \mathbf{H}_k^T \boldsymbol{\varphi}_{11} + \mathbf{P}_{xx,k}|_{k-1} \mathbf{L}_k^T \boldsymbol{\varphi}_{21} \\ &= \mathbf{P}_{xx,k}|_{k-1} \mathbf{H}_k^T (\boldsymbol{\mu}_{11}^{-1} - \boldsymbol{\varphi}_{12} \boldsymbol{\mu}_{21} \boldsymbol{\mu}_{11}^{-1}) \\ &\quad + \mathbf{P}_{xx,k}|_{k-1} \mathbf{L}_k^T (-\boldsymbol{\varphi}_{22} \boldsymbol{\mu}_{21} \boldsymbol{\mu}_{11}^{-1}) \\ &= \mathbf{P}_{xx,k}|_{k-1} \mathbf{H}_k^T \boldsymbol{\mu}_{11}^{-1} + \mathbf{P}_{xx,k}|_{k-1} (\mathbf{H}_k^T \boldsymbol{\mu}_{11}^{-1} \boldsymbol{\mu}_{12} - \mathbf{L}_k^T) \\ &\quad \times (\boldsymbol{\varphi}_{22} \boldsymbol{\mu}_{21} \boldsymbol{\mu}_{11}^{-1}) \\ &= \mathbf{P}_{xx,k}|_{k-1} \mathbf{H}_k^T \boldsymbol{\mu}_{11}^{-1} + \mathbf{P}_{xx,k}|_{k-1} (\mathbf{H}_k^T \boldsymbol{\mu}_{11}^{-1} \boldsymbol{\mu}_{12} - \mathbf{L}_k^T) \\ &\quad \cdot ((\boldsymbol{\mu}_{22} - \boldsymbol{\mu}_{21} \boldsymbol{\mu}_{11}^{-1} \boldsymbol{\mu}_{12})^{-1} \boldsymbol{\mu}_{21} \boldsymbol{\mu}_{11}^{-1}) \\ &= \mathbf{P}_{xx,k}|_{k-1} \mathbf{H}_k^T \left( \mathbf{I} + \mathbf{H}_k \mathbf{P}_{xx,k}|_{k-1} \mathbf{H}_k^T \right)^{-1} \\ &\quad + \mathbf{P}_{xx,k}|_{k-1} \left( \mathbf{H}_k^T \boldsymbol{\mu}_{11}^{-1} \boldsymbol{\mu}_{12} - \mathbf{L}_k^T \right) \\ &\quad \cdot \left( \boldsymbol{\mu}_{22} - \boldsymbol{\mu}_{21} \boldsymbol{\mu}_{11}^{-1} \boldsymbol{\mu}_{12} \right)^{-1} \mathbf{L}_k \mathbf{P}_{xx,k}|_{k-1} \mathbf{H}_k^T \\ &\quad \times \left( \mathbf{I} + \mathbf{H}_k \mathbf{P}_{xx,k}|_{k-1} \mathbf{H}_k^T \right)^{-1} \end{aligned} \quad (24)$$

Substituting  $\mathbf{K}_k = \mathbf{P}_{xx,k}|_{k-1} \mathbf{H}_k^T \left( \mathbf{I} + \mathbf{H}_k \mathbf{P}_{xx,k}|_{k-1} \mathbf{H}_k^T \right)^{-1}$  into Equation (24), and  $\mathbf{S}_M$  can be further simplified as:

$$\begin{aligned} \mathbf{S}_M &= \mathbf{K}_k + \mathbf{P}_{xx,k}|_{k-1} (\mathbf{H}_k^T \boldsymbol{\mu}_{11}^{-1} \boldsymbol{\mu}_{12} - \mathbf{L}_k^T) \\ &\quad \times \left( \boldsymbol{\mu}_{22} - \boldsymbol{\mu}_{21} \boldsymbol{\mu}_{11}^{-1} \boldsymbol{\mu}_{12} \right)^{-1} \mathbf{L}_k \mathbf{K}_k \\ &= \left\{ \mathbf{I} + (\mathbf{K}_k \mathbf{H}_k - \mathbf{I}) \mathbf{P}_{xx,k}|_{k-1} \mathbf{L}_k^T \left[ -\xi^2 \mathbf{I} + \mathbf{L}_k (\mathbf{I} - \mathbf{K}_k \mathbf{H}_k) \right. \right. \\ &\quad \left. \left. \mathbf{P}_{xx,k}|_{k-1} \mathbf{L}_k^T \right]^{-1} \mathbf{L}_k \right\} \mathbf{K}_k \end{aligned} \quad (25)$$

By defining  $\boldsymbol{\vartheta}_k = (\mathbf{I} - \mathbf{K}_k \mathbf{H}_k) \mathbf{P}_{xx,k}|_{k-1} \mathbf{L}_k^T [-\xi^2 \mathbf{I} + \mathbf{L}_k (\mathbf{I} - \mathbf{K}_k \mathbf{H}_k) \mathbf{P}_{xx,k}|_{k-1} \mathbf{L}_k^T]^{-1} \mathbf{L}_k$ , Equation (25) can be simplified as:

$$\mathbf{S}_M = (\mathbf{I} - \boldsymbol{\vartheta}_k) \mathbf{K}_k \quad (26)$$

Similarly,  $\mathbf{S}_N$  can be simplified as:

$$\begin{aligned} \mathbf{S}_N &= \mathbf{P}_{xx,k}|_{k-1} \mathbf{H}_k^T \boldsymbol{\varphi}_{12} + \mathbf{P}_{xx,k}|_{k-1} \mathbf{L}_k^T \boldsymbol{\varphi}_{22} \\ &= \left[ \mathbf{I} - \mathbf{P}_{xx,k}|_{k-1} \mathbf{H}_k^T \left( \mathbf{I} + \mathbf{H}_k \mathbf{P}_{xx,k}|_{k-1} \mathbf{H}_k^T \right)^{-1} \mathbf{H}_k \right] \\ &\quad \times \mathbf{P}_{xx,k}|_{k-1} \mathbf{L}_k^T \\ &\quad \cdot \left[ -\xi^2 \mathbf{I} + \mathbf{L}_k \left( \mathbf{I} - \mathbf{P}_{xx,k}|_{k-1} \mathbf{H}_k^T \left( \mathbf{I} + \mathbf{H}_k \mathbf{P}_{xx,k}|_{k-1} \right. \right. \right. \\ &\quad \left. \left. \times \mathbf{H}_k^T \right)^{-1} \mathbf{H}_k \right) \mathbf{P}_{xx,k}|_{k-1} \mathbf{L}_k^T \right]^{-1} \\ &= (\mathbf{I} - \mathbf{K}_k \mathbf{H}_k) \mathbf{P}_{xx,k}|_{k-1} \mathbf{L}_k^T \left[ -\xi^2 \mathbf{I} + \mathbf{L}_k (\mathbf{I} - \mathbf{K}_k \mathbf{H}_k) \right. \\ &\quad \left. \times \mathbf{P}_{xx,k}|_{k-1} \mathbf{L}_k^T \right]^{-1} \end{aligned} \quad (27)$$

Finally, by substituting the simplified  $S_{\infty,k} = [S_M S_N]$  into Equation (19),  $P_k$  can be expressed as follows:

$$P_k = P_{xx,k|k-1} - (I - \vartheta_k) K_k H_k P_{xx,k|k-1} - \vartheta_k P_{xx,k|k-1} \quad (28)$$

Therefore, the implementation of the UT-H $\infty$  filter algorithm can be presented as follows:

(1) Initialization:

$$\begin{aligned} \hat{X}_0 &= E[X_0] \\ P_0 &= E\left[(X_0 - \hat{X}_0)(X_0 - \hat{X}_0)^T\right] \end{aligned} \quad (29)$$

(2) Time updating:

$$\begin{aligned} X_0 &= \hat{X}_{k-1} \\ X_i &= [\hat{X}_{k-1}]_N + \sqrt{(N + \gamma) P_{k-1i}} \quad i = 1, 2, \dots, N \\ X_i &= [\hat{X}_{k-1}]_N - \sqrt{(N + \gamma) P_{k-1i-N}} \\ &\quad i = N + 1, N + 2, \dots, 2N \\ X_{k|k-1} &= f(X_{k-1}) \\ \hat{X}_{k|k-1} &= \sum_{i=0}^{2n} W_i^m X_{i,k|k-1} \\ P_{xx,k|k-1} &= \sum_{i=0}^{2n} W_i^c \left( X_{i,k|k-1} - \hat{X}_{k|k-1} \right) \\ &\quad \times \left( X_{i,k|k-1} - \hat{X}_{k|k-1} \right)^T + \Gamma_{k-1} \Gamma_{k-1}^T \end{aligned} \quad (30)$$

(3) Measurement updating:

$$\begin{aligned} K_k &= P_{xx,k|k-1} H_k^T \left( H_k P_{xx,k|k-1} H_k^T + I \right)^{-1} \\ \hat{X}_k &= \hat{X}_{k|k-1} + K_k \left( Y_k - H_k \hat{X}_{k|k-1} \right) \\ \vartheta_k &= (I - K_k H_k) P_{xx,k|k-1} L_k^T \\ &\quad \times \left[ -\xi^2 I + L_k (I - K_k H_k) P_{xx,k|k-1} L_k^T \right]^{-1} L_k \\ P_k &= P_{xx,k|k-1} - (I - \vartheta_k) K_k H_k P_{xx,k|k-1} - \vartheta_k P_{xx,k|k-1} \end{aligned} \quad (31)$$

The parameters for calculating the sigma-points are given as follows:

$$\begin{aligned} \gamma &= \alpha^2 (N + \kappa) - N \\ W_0^m &= \gamma / (N + \gamma) \\ W_0^c &= \gamma / (N + \gamma) + (1 - \alpha^2 + \beta) \\ W_i^m &= W_i^c = 1/2 (N + \gamma) \quad i = 1, 2, \dots, 2N \end{aligned} \quad (32)$$

Compared with simplified UKF algorithm, the UT-H $\infty$  filter algorithm adds robustness when calculating  $P_k$ . After giving the value of the robustness factor  $\xi$ , the matrix  $\vartheta_k$  can be calculated. Then,  $P_k$  can be adjusted by  $\vartheta_k$ , and the filtering gain  $K_k$  can be adjusted by  $P_k$ . Therefore, the robustness of the system can be improved.

## B. ADAPTIVE UT-H $\infty$ FILTER

From the above analysis, robustness is added when calculating  $P_k$  in the UT-H $\infty$  filter, and the  $P_k$  is eventually adjusted by the robustness factor  $\xi$ . Hence, the robustness factor  $\xi$  is crucial to the robustness of the UT-H $\infty$  filter. When the value of robustness factor  $\xi$  is small, the robustness of the UT-H $\infty$  filter is strong, but the filtering accuracy decreases. When the value of the robustness factor  $\xi$  is large, the robustness of the UT-H $\infty$  filter declines, and the filtering accuracy increases. However, in each application, the value of the robustness factor  $\xi$  in the UT-H $\infty$  filter has to be artificially chosen by experience, and once selected, the value of  $\xi$  is a constant [19], [27], [31]. This will require significant time in determining the value of  $\xi$  before using the UT-H $\infty$  filter, and the selected value of  $\xi$  is not guaranteed to be optimal in various situations [7], [30]. Moreover, there are always external disturbances in a real system, and the disturbances are time-varying and uncertain [17], [18]. If the value of  $\xi$  is fixed, the dynamic balance between robustness and filtering accuracy may not be maintained, and the filtering estimation error may increase when there are large disturbances in the system. To solve this problem, this paper proposes an adaptive UT-H $\infty$  filter which can dynamically adjust the value of  $\xi$  under uncertain external disturbances.

In a real system, the filter innovation  $\tau_k$  can reflect the extent of the uncertain external disturbances. The filter innovation  $\tau_k$  has a positive correlation with the external disturbances, and it can be written as follows:

$$\tau_k = Y_k - H_k \hat{X}_{k|k-1} \quad (33)$$

Therefore, the quadratic sum of the filter innovation  $\tau_k$  can be written as  $\tau_k^T \tau_k$ , which is the actual estimation error. The theoretical estimation error is expressed as  $E[\tau_k^T \tau_k]$ . The filter innovation is a zero mean Gaussian white noise sequence under ideal conditions. However, the changes of the system model or the anomaly of observed states will change the statistical properties of the filter innovation. If the value of  $\tau_k^T \tau_k$  becomes large, it indicates that the system undergoes a significant external disturbance, and the robustness factor  $\xi$  should be decreased to improve the robustness of the system. If the value of  $\tau_k^T \tau_k$  becomes small, it indicates that there is a small external disturbance at this moment, and the robustness factor  $\xi$  should be increased to improve the filtering accuracy [7]. Hence, the robustness factor  $\xi$  is negatively proportional to the value of  $\tau_k^T \tau_k$ .

*Theorem 2 ([33]): Assuming that  $U$  and  $V$  are two  $n$ -order Hermitian matrices,  $U > 0$ ,  $V \geq 0$ , then  $U > V$  is if and only if  $\lambda_{\max}(VU^{-1}) < 1$ . Here,  $\lambda_{\max}(U)$  represents the maximum eigenvalue of matrix  $U$ .*

Based on the Theorem 2, the conditional Equation (15) of the UT-H $\infty$  filter can be transformed to the following form:

$$\xi^2 > \lambda_{\max}(L_k^T L_k (P_k^{-1} + H_k^T H_k)^{-1}) \quad (34)$$

Then, the value of  $\xi$  can be represented as:

$$\xi = (1 + \rho) \cdot [\lambda_{\max}(L_k^T L_k (P_k^{-1} + H_k^T H_k)^{-1})]^{1/2} \quad (35)$$

In Equation (36), the coefficient  $\rho$  is greater than 0. Based on the above analysis, the value of the robustness factor  $\xi$  is proportional to  $\tau_k^T \tau_k$ . Then, the relationship between the coefficient  $\rho$  and  $\tau_k^T \tau_k$  can be established as follows:

$$\rho = \frac{\partial}{\sqrt{\frac{\tau_k^T \tau_k}{N}}} \quad (37)$$

In the above Equation,  $\partial$  is a correlation coefficient and  $\partial > 0$ . The value of  $\partial$  is determined by the experiment with a real system.  $N$  is the dimension of the system states. In a real system, the values of  $\kappa$  and  $N$  are constants and remain unchanged. Consequently, the value of the coefficient  $\rho$  only has a relationship with  $\tau_k^T \tau_k$ . When  $\tau_k^T \tau_k$  becomes large, the value of coefficient  $\rho$  decreases, so the value of  $\xi$  will decrease to improve the robustness of the system. Conversely, when  $\tau_k^T \tau_k$  becomes small, the value of coefficient  $\rho$  increases; then, the value of  $\xi$  will increase to improve the filtering accuracy [7]. Therefore, the value of  $\xi$  can be adaptively adjusted when the external environment changes, and the robustness and the filtering accuracy achieve a dynamic balance under uncertain disturbances.

#### IV. TRANSFER ALIGNMENT MODEL

##### A. SINS NONLINEAR ERROR DYNAMICS MODEL

This paper defines ‘‘east–north–up (ENU)’’ as the navigation frame, and ‘‘right–forward–up’’ as the body frame. Because of various error sources, rotation error exists between the SINS' calculated mathematical platform  $n'$  frame and the ideal navigation  $n$  frame. The ideal navigation  $n$  frame can be converted to the SINS' calculated mathematical platform  $n'$  by three rotations. The three rotational angles  $\phi_x, \phi_y, \phi_z$  are called as Euler platform error angles, and  $\phi = [\phi_x \ \phi_y \ \phi_z]^T$ . Then, the transformation matrix from the  $n$  frame to the  $n'$  frame can be expressed as [10]:

$$\begin{aligned} C_n^{n'} &= C_{\phi_y} C_{\phi_x} C_{\phi_z} \\ &= \begin{bmatrix} c\phi_y c\phi_z - s\phi_y s\phi_x s\phi_z & c\phi_y s\phi_z + s\phi_y s\phi_x c\phi_z & -s\phi_y c\phi_x \\ -c\phi_x s\phi_z & c\phi_x c\phi_z & s\phi_x \\ s\phi_y c\phi_z + c\phi_y s\phi_x s\phi_z & s\phi_y s\phi_z - c\phi_y s\phi_x c\phi_z & c\phi_y c\phi_x \end{bmatrix} \end{aligned} \quad (38)$$

where  $s\phi_i$  and  $c\phi_i$  represent  $\sin(\phi_i)$  and  $\cos(\phi_i)$  ( $i = x, y, z$ ), respectively.

The mathematical relationship between the output of the accelerometer and the velocity of the carrier can be established by the velocity error equation, which can be written in the navigation frame  $n$  as [34]:

$$\delta \dot{V}^n = (C_n^{n'} - I) f^n - (2\delta\omega_{ie}^n + \omega_{en}^n) \times \delta V^n - (2\delta\omega_{ie}^n + \delta\omega_{en}^n) \times V^n + C_b^n \nabla^b \quad (39)$$

where  $\delta V^n = [\delta V_E \ \delta V_N \ \delta V_U]^T$  is the velocity error;  $\delta \dot{V}^n$  is the derivative of  $\delta V^n$ ;  $f^n = [f_E \ f_N \ f_U]^T$  is the specific force vector;  $\nabla^b = [\nabla_x \ \nabla_y \ \nabla_z]^T$  is the three-axis accelerometer bias in the body frame;  $C_b^n$  denotes

the SINS attitude matrix from the body frame to the navigation frame, which is described as  $C_b^n = [T_{ij}]_{3 \times 3}$ ;  $\omega_{ie}^n$  is the Earth's rotation rate;  $\delta\omega_{ie}^n$  is the derivative of  $\omega_{ie}^n$ ;  $\omega_{en}^n$  is the angular rate of the earth frame relative to the navigation frame; and  $\delta\omega_{en}^n$  is the derivative of  $\omega_{en}^n$ . The concrete expressions for  $\omega_{ie}^n$  and  $\omega_{en}^n$  are presented by Equations (40) and (41), respectively:

$$\omega_{ie}^n = \begin{bmatrix} 0 & \omega_{ie} \cos L & \omega_{ie} \sin L \end{bmatrix}^T \quad (40)$$

$$\omega_{en}^n = \begin{bmatrix} -\frac{V_N}{RM} & \frac{V_E}{RN} & \frac{V_E \tan L}{RN} \end{bmatrix}^T \quad (41)$$

where  $L$  is the latitude,  $RM$  is the radius of curvature on the meridian, and  $RN$  is the radius of curvature on the prime vertical.

The SINS' position error equations can be written as [2]:

$$\delta \dot{L} = \frac{\delta V_N}{R_M + h} - \delta h \frac{V_N}{(R_M + h)^2} \quad (42)$$

$$\delta \dot{\lambda} = \frac{\delta V_E}{R_N + h} \sec L + \delta L \frac{V_E}{R_N + h} \tan L \sec L - \delta h \frac{V_E \sec L}{(R_N + h)^2} \quad (43)$$

$$\delta \dot{h} = \delta V_U \quad (44)$$

where  $\delta L, \delta \lambda$  and  $\delta h$  are the latitude error, longitude error and height error, respectively.

By defining the angular rate of the  $n$  frame relative to the  $n'$  frame as  $\omega_{nn'}^n$ , the relationship between  $\omega_{nn'}^n$  and the Euler platform error angle  $\phi$  can be obtained:

$$\omega_{nn'}^n = C_{\phi_y} C_{\phi_x} \begin{bmatrix} 0 \\ 0 \\ \dot{\phi}_z \end{bmatrix} + C_{\phi_y} \begin{bmatrix} \dot{\phi}_x \\ 0 \\ 0 \end{bmatrix} + \begin{bmatrix} 0 \\ \dot{\phi}_y \\ 0 \end{bmatrix} = C_\omega \begin{bmatrix} \dot{\phi}_x \\ \dot{\phi}_y \\ \dot{\phi}_z \end{bmatrix} \quad (45)$$

From Equation (45), the differential equation of the Euler platform error angle can be written as follows:

$$\dot{\phi} = C_\omega^{-1} \omega_{nn'}^n \quad (46)$$

where

$$C_\omega = \begin{bmatrix} c\phi_y & 0 & -s\phi_y c\phi_x \\ 0 & 1 & s\phi_x \\ s\phi_y & 0 & c\phi_y c\phi_x \end{bmatrix} \quad (47)$$

$$C_\omega^{-1} = \frac{1}{c\phi_x} \begin{bmatrix} c\phi_y c\phi_x & 0 & s\phi_y c\phi_x \\ s\phi_y s\phi_x & c\phi_x & -c\phi_y s\phi_x \\ -s\phi_y & 0 & c\phi_y \end{bmatrix} \quad (48)$$

The instrument angular velocity and gyro bias have influence on the SINS' attitude angle error, and the gyro bias leads to the increasing of attitude angle error. The concrete expressions of attitude error equation can be written in the navigation frame  $n$  as [34]:

$$\dot{\phi}^n = C_\omega^{-1} [(I - C_n^{n'}) \omega_{in}^n + C_n^{n'} \delta \omega_{in}^n - C_b^n \mathbf{e}^b] \quad (49)$$

where  $\phi^n = [\phi_E \ \phi_N \ \phi_U]^T$  is the calculated platform's attitude angle error;  $\mathbf{e}^b = [\varepsilon_x \ \varepsilon_y \ \varepsilon_z]^T$  denotes the three-axis gyro drift in the body frame;  $C_b^n = C_n^{n'} C_b^n$ ;  $\omega_{in}^n$

denotes the angular rate of the inertial frame relative to the navigation frame;  $\delta\omega_{in}^n$  denotes the derivative of  $\omega_{in}^n$ . Moreover,  $\omega_{in}^n$  can be expressed as follows:

$$\omega_{in}^n = \omega_{ie}^n + \omega_{en}^n \quad (50)$$

Generally, the three-axis accelerometer biases and the three-axis gyro drifts are not considered to be time-varying, that is [35]:

$$\dot{\nabla}^b = 0 \quad (51)$$

$$\dot{\epsilon}^b = 0 \quad (52)$$

Based on the above error equations, twelve dimensional states are chosen to set up state equations. In addition, the system states are presented as follows:

$$\mathbf{X}(t) = [\delta L, \delta\lambda, \delta V_E, \delta V_N, \phi_E, \phi_N, \phi_U, \nabla_x, \nabla_y, \epsilon_x, \epsilon_y, \epsilon_z]^T \quad (53)$$

where  $\delta V_E$  and  $\delta V_N$  are the east and north velocity errors in the navigation frame, respectively;  $\phi_E, \phi_N,$  and  $\phi_U$  are the east, north and azimuth misalignment angles in the navigation frame, respectively;  $\nabla_x$  and  $\nabla_y$  are the right-axis and forward-axis accelerometer biases in the body frame, respectively;  $\epsilon_x, \epsilon_y,$  and  $\epsilon_z$  are the right-axis, forward-axis, and up-axis gyro drifts in the body frame, respectively.

The nonlinear system's state equation can be constructed as follows:

$$\mathbf{X}_k = f(\mathbf{X}_{k-1}) + \mathbf{\Gamma}(\mathbf{X}_{k-1})\mathbf{W}_{k-1} \quad (54)$$

where  $f(\cdot)$  and  $\mathbf{\Gamma}(\cdot)$  are all nonlinear functions,  $\mathbf{X}_{k-1}$  is ( $N \times 1$ ) state estimate,  $\mathbf{X}_k$  is ( $N \times 1$ ) one step predicted state, and variable  $\mathbf{W}_{k-1}$  is process noise.

### B. MEASUREMENT MODEL

In the model of transfer alignment, velocity and attitude matrix differences between M-SINS and S-SINS are chosen as measurement.  $\hat{\mathbf{C}}_{b_m}^n$  and  $\hat{\mathbf{C}}_{b_s}^n$  are defined as the attitude matrix calculated by the M-SINS and the S-SINS respectively.  $b_m$  and  $b_s$  denote the measurement frame of the M-SINS and the S-SINS, respectively. Then, the following matrix can be constructed:

$$\mathbf{M} = \hat{\mathbf{C}}_{b_m}^n (\hat{\mathbf{C}}_{b_s}^n)^T \quad (55)$$

In Equation (55), the second order terms are ignored, and the M-SINS' misalignment angles and the installation error angles between M-SINS and S-SINS are assumed as small angles. Then  $\mathbf{M}$  can be presented as follows:

$$\mathbf{M} = \begin{bmatrix} 1 & -Z_z & Z_y \\ Z_z & 1 & -Z_x \\ -Z_y & Z_x & 1 \end{bmatrix} \approx \mathbf{I} + (\mathbf{Z}_{DCM} \times) \quad (56)$$

where  $\mathbf{Z}_{DCM} = [Z_x \ Z_y \ Z_z]^T$  and  $Z_z = M(2, 1), Z_y = M(1, 3), Z_x = M(3, 2), -Z_z = M(1, 2), -Z_y = M(3, 1),$  and

$-Z_x = M(2, 3)$ . Therefore, the measurement of velocity plus attitude matrix matching can be expressed as follows:

$$\mathbf{Y}(k) = \begin{bmatrix} \delta V_E \\ \delta V_N \\ Z_x \\ Z_y \\ Z_z \end{bmatrix} = \begin{bmatrix} \tilde{V}_E^s - V_E^m \\ \tilde{V}_N^s - V_N^m \\ 1/2 [M(3, 2) - M(2, 3)] \\ 1/2 [M(1, 3) - M(3, 1)] \\ 1/2 [M(2, 1) - M(1, 2)] \end{bmatrix} \quad (57)$$

where  $\mathbf{Y}(k)$  is the measurement matrix;  $\delta V_E$  and  $\delta V_N$  are the M-SINS' east velocity error and north velocity error, respectively;  $\tilde{V}_E^s$  and  $\tilde{V}_N^s$  are the S-SINS' east velocity and north velocity, respectively;  $V_E^m$  and  $V_N^m$  are the M-SINS' east velocity and north velocity, respectively.

The system's measurement equation can be presented as follows:

$$\mathbf{Y}_k = \mathbf{H}_k \mathbf{X}_k + \mathbf{V}_k \quad (58)$$

where  $\mathbf{V}_k$  is the measurement noise,  $\mathbf{H}_k$  is the measurement matrix and

$$\mathbf{H}(k) = \begin{bmatrix} \mathbf{0}_{2 \times 2} & \mathbf{0}_{2 \times 5} & \mathbf{0}_{2 \times 5} \\ \mathbf{0}_{5 \times 2} & \mathbf{I}_{5 \times 5} & \mathbf{0}_{5 \times 5} \\ \mathbf{0}_{5 \times 2} & \mathbf{0}_{5 \times 5} & \mathbf{0}_{5 \times 5} \end{bmatrix} \quad (59)$$

### C. SENSOR ERROR COMPENSATION MODEL

When conducting the transfer alignment, the sensor errors of gyros and accelerometers play an important role in the alignment accuracy [1], [5]. The subsequent navigation accuracy is also seriously influenced by the sensor errors. Consequently, calibrating and compensating the sensor errors of gyros and accelerometers is necessary. The gyro drift consists of three parts, and it can be expressed as follows:

$$\epsilon_i^b = \epsilon_{bi}^b + \epsilon_{ri}^b + \omega_{gi}^b \quad (i = x, y, z) \quad (60)$$

where  $\epsilon_i^b$  is gyro drift,  $\epsilon_{bi}^b$  is random constant drift,  $\epsilon_{ri}^b$  is random slowly varying drift, and  $\omega_{gi}^b$  is varying drift that is uncorrelated with itself. In the three parts of gyro drift,  $\epsilon_{bi}^b$  is a random constant each time the gyro starts,  $\epsilon_{ri}^b$  is a slowly changing quantity, and  $\omega_{gi}^b$  is a rapidly changing quantity. For the configuration envisioned for this study,  $\epsilon_{bi}^b$  is the main error source for the gyro drift. This study uses the adaptive UT-H $\infty$  filter to estimate  $\epsilon_{bi}^b$ , and the compensated gyro drift can be written as:

$$\epsilon_{i\_cpt}^b = \epsilon_{bi}^b + \epsilon_{ri}^b + \omega_{gi}^b - \epsilon_{bi\_clt}^b \quad (i = x, y, z) \quad (61)$$

where  $\epsilon_{i\_cpt}^b$  is the compensated gyro drift and  $\epsilon_{bi\_clt}^b$  is the estimated random constant drift.

The accelerometer bias consists of two parts, and it can be expressed as follows:

$$\nabla_i^b = \nabla_{bi}^b + \omega_{ai}^b \quad (i = x, y, z) \quad (62)$$

where  $\nabla_i^b$  is the accelerometer bias,  $\nabla_{bi}^b$  is random constant bias, and  $\omega_{ai}^b$  is random rapidly varying bias. In the two parts of the accelerometer bias,  $\nabla_{bi}^b$  is a random constant each time the accelerometer starts, and  $\omega_{ai}^b$  is a rapidly changing quantity. For the configuration envisioned for this study,

**TABLE 1. Specifications of the inertial sensors (1 $\sigma$ ).**

Sensor Error	Gyro Bias		Accelerometer Bias	
	Constant ( $^{\circ}/h$ )	Noise ( $^{\circ}/h^{1/2}$ )	Constant ( $\mu g$ )	Noise ( $\mu g/Hz^{1/2}$ )
M-SINS	0.02	0.005	50	20
S-SINS	1.0	0.25	100	40

$\nabla_{bi}^b$  is the main error source for the accelerometer bias. This study uses the adaptive UT-H $\infty$  filter to estimate  $\nabla_{bi}^b$ , and the compensated accelerometer bias can be written as:

$$\nabla_{i\_cpt}^b = \nabla_{bi}^b + \omega_{ai}^b - \nabla_{bi\_clt}^b \quad (i = x, y, z) \quad (63)$$

where  $\nabla_{i\_cpt}^b$  is the compensated accelerometer bias and  $\nabla_{bi\_clt}^b$  is the estimated random constant bias.

## V. EXPERIMENTAL RESULTS AND DISCUSSIONS

### A. EXPERIMENTAL SETTINGS

To verify the proposed adaptive UT-H $\infty$  filtering method, this study designs a vehicle transfer alignment experiment in an actual system. The vehicle experiment was carried out outdoors in Beijing. The approximate location is east longitude 116 $^{\circ}$  and north latitude 39 $^{\circ}$ . The experimental equipment included a test vehicle, navigation computer, M-SINS, S-SINS, power source and communication lines. The three-axis gyro random constant drifts of M-SINS and S-SINS were 0.02  $^{\circ}/h$  and 1  $^{\circ}/h$ , respectively. The three-axis accelerometer random constant biases of M-SINS and S-SINS were 50  $\mu g$  and 100  $\mu g$ , respectively. The accuracy of M-SINS is two orders of magnitude higher than the S-SINS. The detailed specifications of the inertial sensors are listed in Table 1. The M-SINS provides the reference baseline information, including attitude angles, velocities, and position during the process of transfer alignment. The update frequencies of M-SINS and S-SINS were all 200 Hz, and the cycle of attitude solution was 5 ms. To intentionally add large initial attitude errors, the S-SINS' heading angle error, pitch angle error, and roll angle error were set to increase by 10 $^{\circ}$ , 1 $^{\circ}$ , 1 $^{\circ}$ , respectively. The whole trajectory of the vehicle transfer alignment experiment is shown in Figure 1.

When the test vehicle ran on the road, the power source powered the M-SINS and S-SINS, and they began to work. Before transfer alignment, the M-SINS firstly completed self-alignment. Then, the real-time data that were output by M-SINS and S-SINS were transmitted to the navigation computer by communication lines. In this transfer alignment experiment, the navigation computer recorded the sensor data for subsequent processing. First, the vehicle experiment spent 350 s on the transfer alignment of S-SINS. Then, after 350 s, the S-SINS started pure inertial navigation for 600 s. During the whole process, the test vehicle ran randomly on the road. Figure 2 shows the heading angle, pitch angle and roll angle

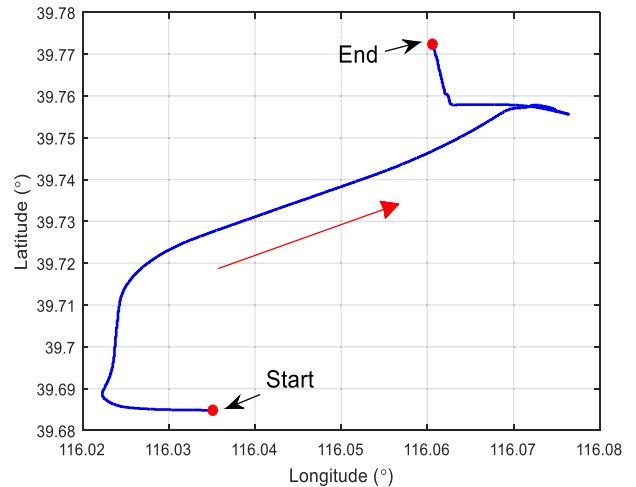


**FIGURE 1. The trajectory of the vehicle transfer alignment experiment.**

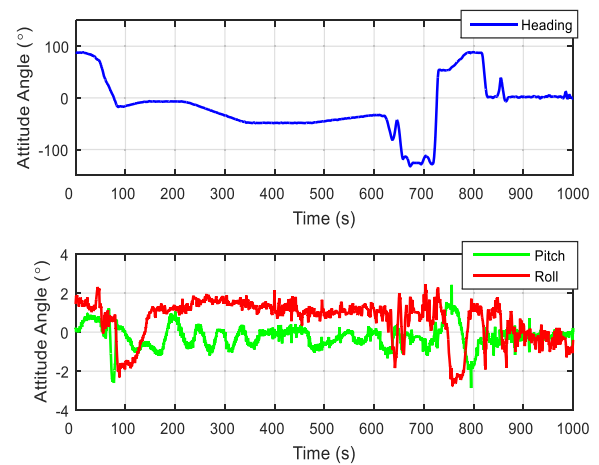


**FIGURE 2. The attitude curves of master SINS (M-SINS).**

of the M-SINS in the whole experiment. The heading angle fluctuates between  $-130^{\circ}$  and  $100^{\circ}$ , and the attitude angles change with the road surface in the experiment.

The M-SINS' east velocity and north velocity are presented in Figure 3. The east velocity and north velocity fluctuate between  $-20$  m/s and  $20$  m/s, and both of them change randomly during the experiment.

### B. EXPERIMENTAL RESULTS AND DISCUSSIONS

In the vehicle transfer alignment experiment, the transfer alignment accuracy is positive with the pure inertial navigation accuracy. And the optimal value of  $\vartheta$  can be chosen by comparing the position errors in pure inertial navigation using different values of  $\vartheta$ . Figure 4 shows the position errors by using different values of  $\vartheta$ . It can be seen from Figure 4 that when the value of  $\vartheta$  is set as 1.5, the position error in pure inertial navigation is smaller compared with that when the value of  $\vartheta$  is bigger or smaller than 1.5. Therefore, the value of  $\vartheta$  was set as 1.5 in the experiment. Since the external disturbances in specific application scenarios are in certain



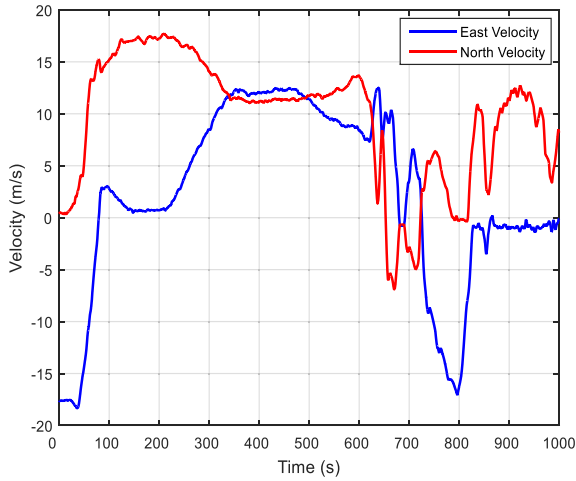


FIGURE 3. The east velocity and north velocity of M-SINS.

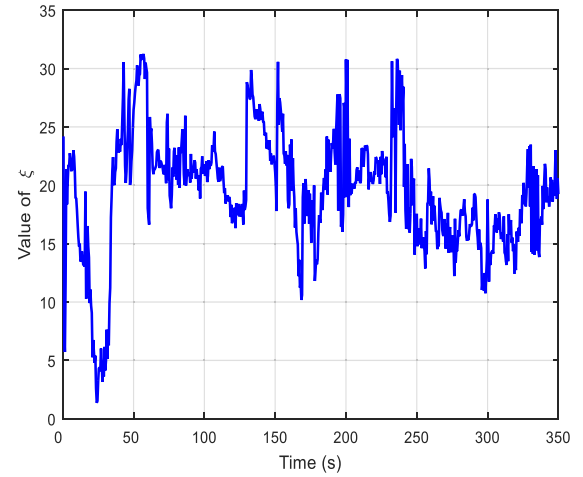


FIGURE 5. The value of robustness factor in the adaptive UT-H $\infty$  filter.

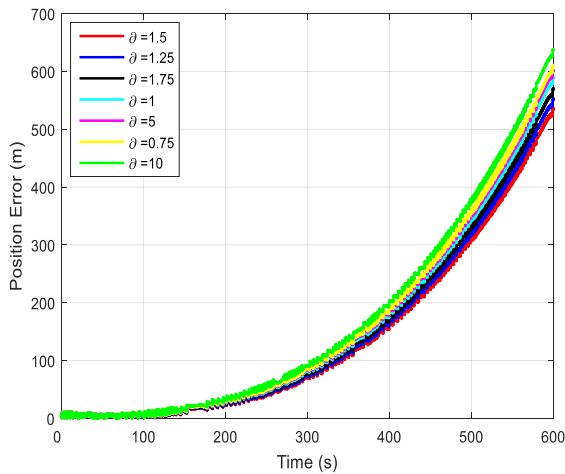


FIGURE 4. The curves of position errors in pure inertial navigation by using different values of  $\Delta$ .

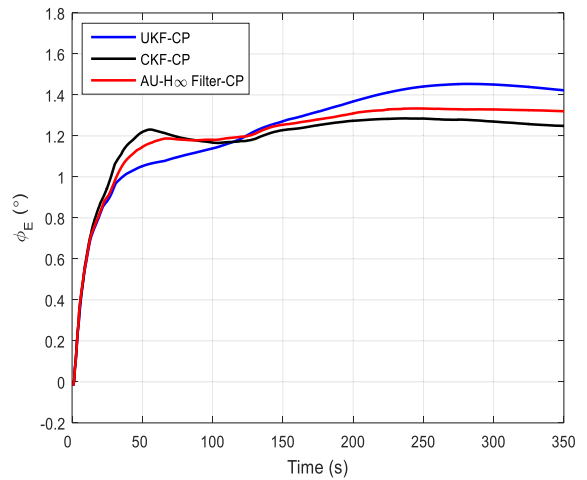


FIGURE 6. The estimation curves of the east misalignment angles. CP denotes “compensate gyro’s drift and accelerometer’s bias”.

range respectively, the value of  $\Delta$  only needs to be set once in each application scenario.

When conducting the transfer alignment experiment, the robustness factor of the proposed adaptive UT-H $\infty$  filter was adjusted adaptively with the change of the unknown external environment. If the system is affected by large external disturbances, the robustness factor will decrease to enhance the robustness of the system. If the system is affected by small external disturbances, the robustness factor will increase to improve the system’s accuracy. For the process of transfer alignment, the change of the robustness factor  $\xi$  is shown in Figure 5.

To compare the transfer alignment effect under different filtering methods, UKF, CKF, and the adaptive UT-H $\infty$  filter were separately applied in the actual experiment. Figures 6–8 show the change of east misalignment angle, north misalignment angle, and azimuth misalignment angle when using the different filtering methods.

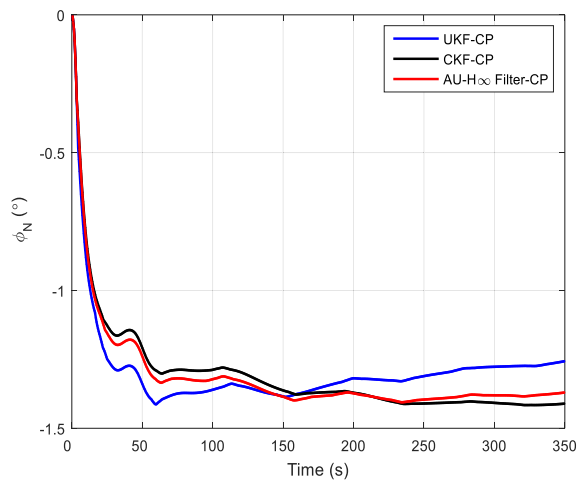


FIGURE 7. The estimation curves of the north misalignment angles.

In the figures, the blue lines represent the estimation curves of the UKF, the black lines represent the estimation curves of the CKF, and the red lines represent the estimation

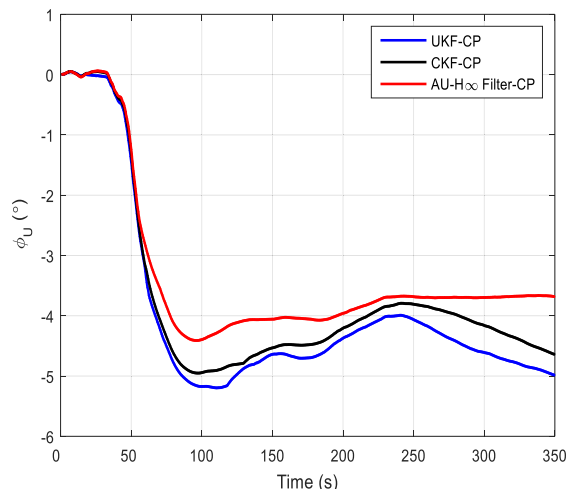


FIGURE 8. The estimation curves of the azimuth misalignment angles.

curves of the adaptive UT-H $\infty$  filter. Figure 6 shows the estimation curves of the east misalignment angle ( $\phi_E$ ) during the transfer alignment experiment. When using the UKF method, the convergence rate of  $\phi_E$  is slow, and it begins to converge to  $1.4^\circ$  after approximately 250 s. However, there are still fluctuations in the curve after 250 s. When using the CKF method, the estimation curve of  $\phi_E$  has a fast rate of convergence, and it begins to converge to  $1.24^\circ$  after 150 s. There are still fluctuations, but they are smaller than those observed using the UKF method. By contrast, when using the adaptive UT-H $\infty$  filtering method, the estimation curve of  $\phi_E$  also has a fast rate of convergence, and it begins to converge after 180 s. The estimation curve tends to be stable at  $1.32^\circ$  eventually, and the fluctuation is the smallest among the three filtering methods. In other words, the estimation curve obtained by using the adaptive UT-H $\infty$  filtering method is more stable than those obtained using UKF method and CKF method. Since the stability of the estimated misalignment angle is an important criterion to evaluate the accuracy of transfer alignment, it can be verified that the proposed adaptive UT-H $\infty$  filtering method has better alignment performance compared with the other two methods.

Figure 7 shows the estimation curves of the north misalignment angle ( $\phi_N$ ) during the transfer alignment experiment. The convergence rate of  $\phi_N$  determined using the three methods is almost the same. When using the UKF method, the estimation curve of  $\phi_N$  tends to converge after 150 s. However, the value of  $\phi_N$  has the tendency to grow slowly after 150 s, and it fluctuates between  $-1.38^\circ$  and  $-1.26^\circ$ . When using the CKF method, the estimation curve of  $\phi_N$  after 150 s has smaller fluctuations than that produced using the UKF method, and the value of  $\phi_N$  converges to  $-1.41^\circ$ . Comparatively, when using the adaptive UT-H $\infty$  filtering method, the estimation curve of  $\phi_N$  is more stable than those produced using the UKF method and CKF method, and the value of  $\phi_N$  converges to  $-1.37^\circ$ . When using the adaptive UT-H $\infty$  filtering method, the range of fluctuations between

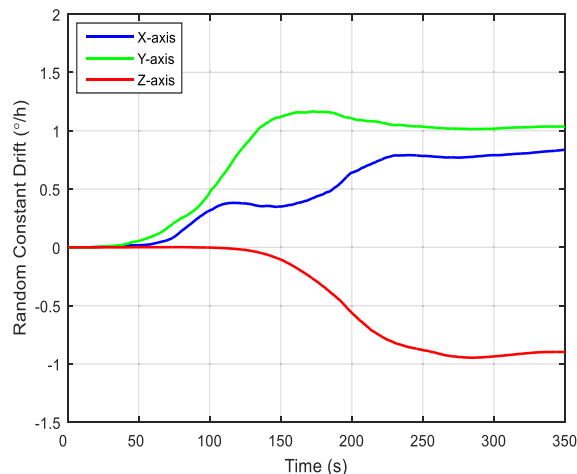


FIGURE 9. The estimation curves of the random constant drift of the gyros in the vehicle transfer alignment experiment.

150 s and 350 s is the smallest among the three methods, which can effectively improve the accuracy of transfer alignment.

The estimation curves of the azimuth misalignment angle ( $\phi_U$ ) produced using the three methods are shown in Figure 8. Due to the theory of SINS' error propagation, the estimation value of  $\phi_U$  has the slowest convergence rate compared to the estimation value of  $\phi_E$  and  $\phi_N$  [35]. When using the UKF method, the estimation curve of  $\phi_U$  fluctuates between  $-5.18^\circ$  and  $-3.99^\circ$ , and the estimation curve of  $\phi_U$  has the fluctuation which is approximately  $1.2^\circ$ . When using the CKF method, the estimation curve of  $\phi_U$  fluctuates between  $-4.95^\circ$  and  $-3.79^\circ$ , and the range of fluctuations is almost the same as that observed using the UKF method. By contrast, when using the adaptive UT-H $\infty$  filtering method, the estimation curve of  $\phi_U$  has small fluctuations after 250 s, and the estimation value of  $\phi_U$  eventually converges to  $-3.68^\circ$ . The stability of the estimated  $\phi_U$  is obviously better than that observed using the other two filtering methods. This verifies that the proposed adaptive UT-H $\infty$  filter has a significant advantage for the SINS' transfer alignment under uncertain external disturbances.

In the process of vehicle transfer alignment, the proposed adaptive UT-H $\infty$  filtering method can simultaneously calibrate the gyro's random constant drifts and the accelerometer's random constant biases online. When the transfer alignment is completed, the random constant errors of the gyros and accelerometers will be compensated for at once. The estimation curves of the gyros' random constant drifts are shown in Figure 9. When calibrating online, the random constant drifts of the X-axis gyro, Y-axis gyro, and Z-axis gyro are  $0.83^\circ/h$ ,  $1.04^\circ/h$ , and  $-0.90^\circ/h$ , respectively. They are approximately within the range of the S-SINS' sensor errors.

The estimation curves of accelerometers' random constant biases during the vehicle transfer alignment experiment are shown in Figure 10. When calibrating online, the

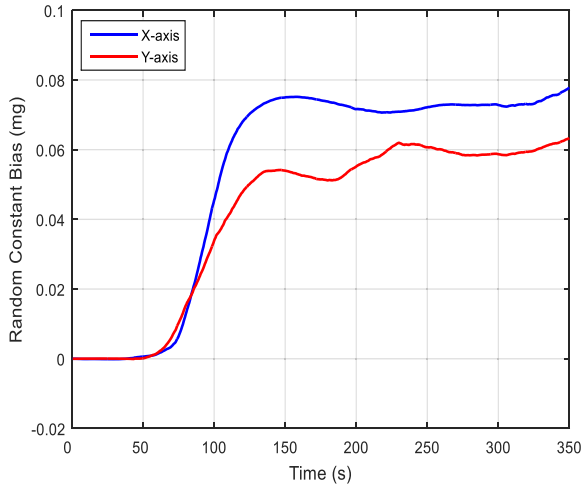


FIGURE 10. The estimation curves of the accelerometers' random constant biases in the vehicle transfer alignment experiment.

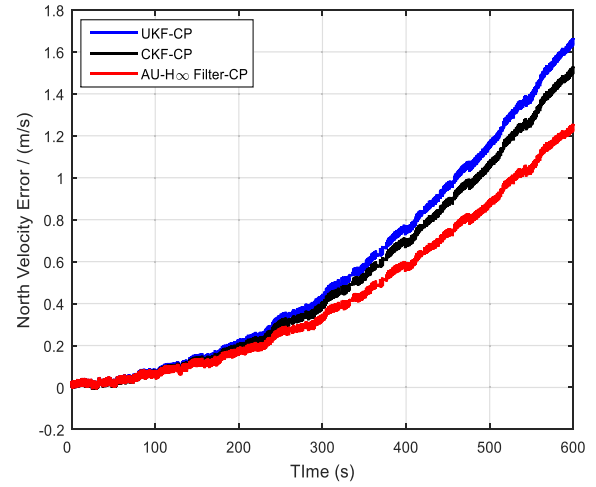


FIGURE 12. The curves of north velocity errors in pure inertial navigation.

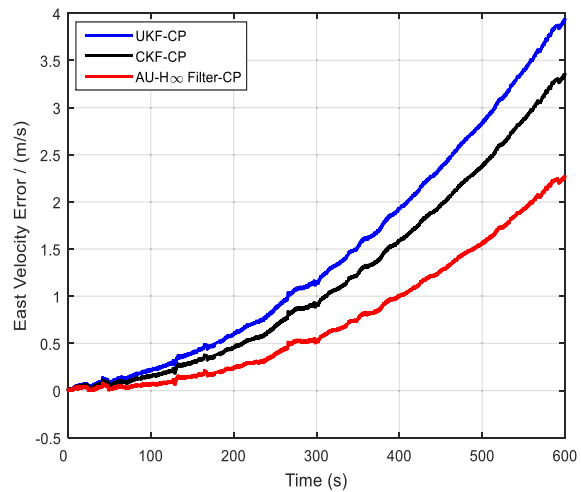


FIGURE 11. The curves of east velocity errors in pure inertial navigation.

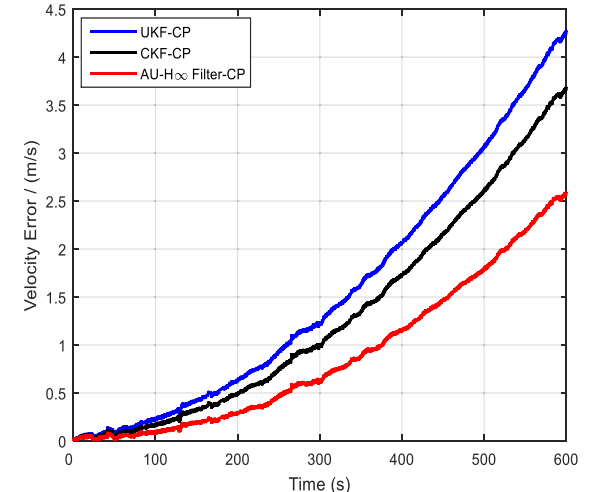


FIGURE 13. The curves of velocity errors in pure inertial navigation.

random constant biases of the X-axis accelerometer and Y-axis accelerometer are approximately 0.07 mg and 0.06 mg, respectively.

With the same sensor errors, the transfer alignment accuracy has a positive correlation with the pure inertial navigation accuracy. The higher the transfer alignment accuracy is, the smaller the pure inertial navigation error is.

Therefore, to further compare the performance of the three filtering methods when conducting the transfer alignment, a pure inertial navigation experiment was conducted immediately after the transfer alignment. The pure inertial navigation experiment lasted 600 s, and Figures 11–13 show the curves of east velocity errors, north velocity errors, and velocity errors when using the three filtering methods. The values of east velocity errors, north velocity errors, and velocity errors after 600 s are listed in Table 2.

From Figure 11–13 and Table 2, the east velocity errors after 600 s of pure inertial navigation determined by using the UKF method, the CKF method, and the adaptive UT-H $\infty$  filtering method are 3.95 m/s, 3.37 m/s, and 2.28 m/s,

TABLE 2. The velocity errors (m/s) after 600 s of pure inertial navigation.

Method	East Velocity Error	North Velocity Error	Velocity Error
UKF-CP	3.95	1.67	4.29
CKF-CP	3.37	1.53	3.68
AU-H $\infty$ Filter-CP	2.28	1.26	2.60

respectively. The north velocity errors determined by using the three filtering methods are 1.67 m/s, 1.53 m/s, and 1.53 m/s, respectively. The velocity errors determined by using the three filtering methods are 4.29 m/s, 3.68 m/s, and 2.60 m/s, respectively. After calculation, it is known that the velocity error determined by using the adaptive UT-H $\infty$  filtering method decreased by 39.39% compared with that determined by using the UKF method and decreased by 29.35% compared with that determined by using the CKF method. This occurs because, under the uncertain external disturbances, the purposed adaptive UT-H $\infty$  filter adds robustness to the system, and the robustness factor  $\xi$  can be

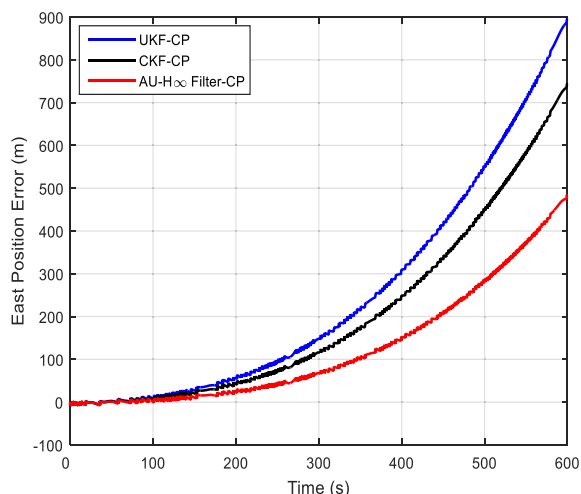


FIGURE 14. The curves of east position errors in pure inertial navigation.

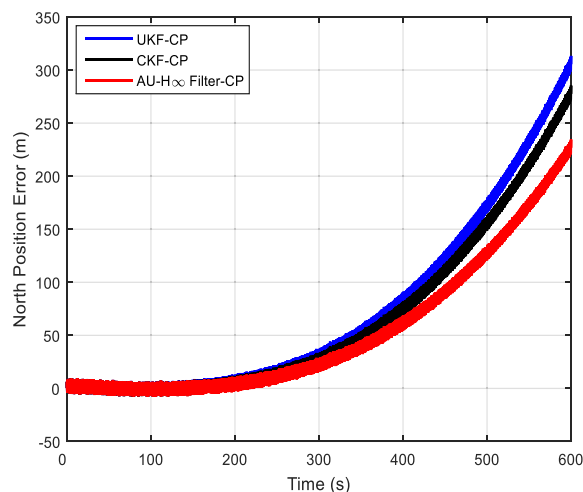


FIGURE 15. The curves of north position errors in pure inertial navigation.

TABLE 3. The position errors (m) after 600 s of pure inertial navigation.

Method	East Position Error	North Position Error	Position Error
UKF-CP	897.15	313.49	950.13
CKF-CP	744.92	285.44	797.76
AU-H $\infty$ Filter-CP	483.46	234.67	537.32

adaptively adjusted with the change of the external disturbance. Accordingly, Figures 14–16 show the curves of the east position errors, the north position errors, and the position errors that occurred when using the three filtering methods. The values of the east position errors, north position errors, and position errors after 600 s of pure inertial navigation are listed in Table 3.

Figure 14–16 and Table 3 show that the east position errors after 600 s of pure inertial navigation using the UKF method, the CKF method, and the adaptive UT-H $\infty$  filtering method are 897.15 m, 744.92 m, and 483.46 m, respectively. The north position errors by using the three filtering methods are 313.49 m, 285.44 m, and 234.67 m, respectively. The total position errors determined by using the three filtering methods are 950.13 m, 797.76 m, and 537.32 m, respectively. Therefore, the position error determined by using the adaptive UT-H $\infty$  filtering method decreased by 43.45% compared with that determined by using the UKF method and decreased by 32.65% compared with that determined by using the CKF method. Since the transfer alignment accuracy finally displays in the pure inertial navigation accuracy, the results of pure inertial navigation adequately reflect the superiority of the proposed adaptive UT-H $\infty$  filtering method. Meanwhile, as the adaptive UT-H $\infty$  filter adds the robustness to resist uncertain external disturbances when conducting the transfer alignment, the bigger the external disturbance is, the more obvious the advantage of the adaptive UT-H $\infty$  filter is.

For the purpose of fully comparing the UKF method, the CKF method and the adaptive UT-H $\infty$  filtering method during the process of transfer alignment under uncertain

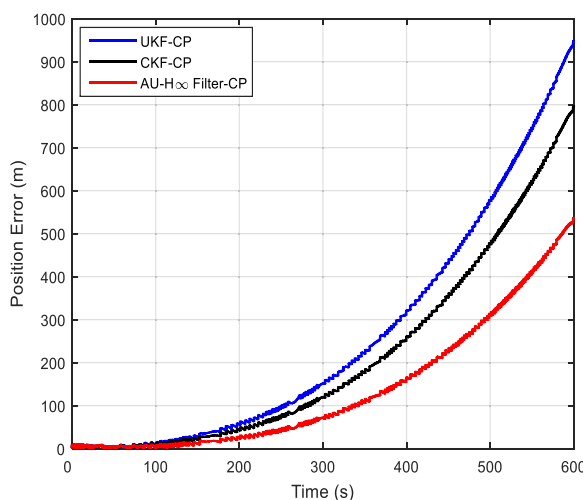


FIGURE 16. The curves of position errors in pure inertial navigation.

disturbances, this study designed a total of 20 groups of vehicle transfer alignment experiments in the real system. The test vehicle's moving trajectories, M-SINS' attitude angles, M-SINS' running speeds and conditions of road surface are entirely different in the 20 groups of experiments. In each experiment, the M-SINS and S-SINS were restarted before working. The time required to conduct the transfer alignment was 350 s and, after transfer alignment, the S-SINS began 600 s of pure inertial navigation. Figure 17 shows the histograms of the position errors after 600 s of pure inertial navigation in 20 groups of vehicle transfer alignment experiments. The position errors in 20 groups of vehicle transfer alignment experiments are listed in Table 4.

Figure 17 and Table 4 show that, in 20 groups of vehicle transfer alignment experiments, the position errors determined by using the adaptive compensation H $\infty$  filter are obviously smaller than those determined by using the UKF method and the CKF method. By calculation, the mean position errors of 20 groups of vehicle transfer alignment

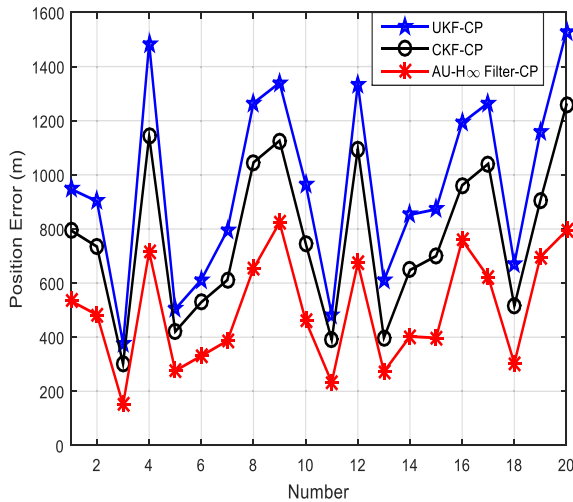


FIGURE 17. The line charts of position errors in 20 groups of vehicle experiments.

TABLE 4. The position errors (m) in 20 groups of vehicle experiments.

Number	UKF-CP	CKF-CP	AU-H $\infty$ Filter-CP
1	950.13	797.76	537.32
2	902.31	734.52	482.88
3	376.35	301.34	150.80
4	1485.08	1142.37	715.98
5	503.69	420.75	275.90
6	612.44	529.49	330.93
7	794.65	611.27	386.88
8	1264.85	1045.71	653.57
9	1339.98	1126.03	823.63
10	966.72	747.18	461.22
11	482.92	389.51	233.24
12	1334.97	1096.42	673.26
13	608.73	397.86	272.51
14	852.83	648.19	402.60
15	872.54	699.83	397.41
16	1192.09	961.37	759.03
17	1265.53	1040.59	622.31
18	670.67	515.90	303.47
19	1159.26	905.67	696.97
20	1529.85	1258.98	793.82

experiments by using the UKF method, the CKF method and the adaptive compensation H $\infty$  filter are 958.280 m, 768.537 m, and 498.687 m, respectively. Consequently, the mean position errors of 20 groups determined by using the adaptive UT-H $\infty$  filtering method were decreased by 47.96% compared with those determined by using the UKF method and were decreased by 35.11% compared with those determined by using the CKF method. The results of the 20 groups of vehicle transfer alignment experiments further illustrate that the proposed adaptive compensation H $\infty$  filter can effectively improve the accuracy of transfer alignment, and it has obvious advantages compared with the UKF method and the CKF method under uncertain external disturbances.

## VI. CONCLUSION

In this work, an adaptive UT-H $\infty$  filter is proposed for SINS transfer alignment with large attitude errors under uncertain disturbances. The adaptive UT-H $\infty$  filter combines the UKF technology and a H $\infty$  filter to increase the robustness of the nonlinear transfer alignment system. The robustness factor of the adaptive UT-H $\infty$  filter is adaptively adjusted with changes of the external disturbances. The nonlinear transfer alignment model, including the SINS nonlinear error model, the velocity plus attitude matrix measurement model and the sensor error compensation model, were established. Moreover, 20 groups of vehicle transfer alignment experiments were conducted to verify the proposed filtering method. The experimental results show that the adaptive UT-H $\infty$  filter has a significant advantage compared with the UKF method and the CKF method under uncertain disturbances. When the external disturbances increase, the advantage of the proposed adaptive UT-H $\infty$  filter will be further presented.

## REFERENCES

- [1] S. Han and J. Wang, "Quantization and colored noises error modeling for inertial sensors for GPS/INS integration," *IEEE Sensors J.*, vol. 11, no. 6, pp. 1493–1503, Jun. 2011.
- [2] X. Gong, H. Liu, J. Fang, and G. Liu, "Multi-node transfer alignment based on mechanics modeling for airborne DPOS," *IEEE Sensors J.*, vol. 18, no. 2, pp. 669–679, Jan. 2018.
- [3] L. Chang, J. Li, and K. Li, "Optimization-based alignment for strap-down inertial navigation system: Comparison and extension," *IEEE Trans. Aerosp. Electron. Syst.*, vol. 52, no. 4, pp. 1697–1713, Aug. 2016.
- [4] Y. Wu and X. Pan, "Velocity/Position integration formula part I: Application to in-flight coarse alignment," *IEEE Trans. Aerosp. Electron. Syst.*, vol. 49, no. 2, pp. 1006–1023, Apr. 2013.
- [5] Y. Wang, F. Sun, Y. Zhang, H. Liu, and H. Min, "Central difference particle filter applied to transfer alignment for SINS on missiles," *IEEE Trans. Aerosp. Electron. Syst.*, vol. 48, no. 1, pp. 375–387, Jan. 2012.
- [6] W.-W. Lyu and X.-H. Cheng, "Novel self-alignment algorithm with unknown latitude for SINS on swing base," *J. Chin. Inertial Technol.*, vol. 25, no. 3, pp. 281–288, 2017.
- [7] W. Lyu, X. Cheng, and J. Wang, "An improved adaptive compensation H $\infty$  filtering method for the SINS' transfer alignment under a complex dynamic environment," *Sensors*, vol. 19, no. 2, p. 401, 2019.
- [8] X. Gong, W. Fan, and J. Fang, "An innovational transfer alignment method based on parameter identification UKF for airborne distributed POS," *Measurement*, vol. 58, pp. 103–114, Dec. 2014.
- [9] S. P. Dmitriyev, O. A. Stepanov, and S. V. Shepel, "Nonlinear filtering methods application in INS alignment," *IEEE Trans. Aerosp. Electron. Syst.*, vol. 33, no. 1, pp. 260–272, Jan. 1997.
- [10] G. Yan, W. Yan, and D. Xu, "Application of simplified UKF in SINS initial alignment for large misalignment angles," *J. Chin. Inertial Technol.*, vol. 16, no. 3, pp. 253–264, 2008.
- [11] W. Li, J. Wang, L. Lu, and W. Wu, "A novel scheme for DVL-aided SINS in-motion alignment using UKF techniques," *Sensors*, vol. 13, no. 1, pp. 1046–1063, Jan. 2013.
- [12] D.-J. Lee, "Nonlinear estimation and multiple sensor fusion using unscented information filtering," *IEEE Signal Process. Lett.*, vol. 15, no. 1, pp. 861–864, 2008.
- [13] K. Hoon Kim, J. Gyu Lee, and C. Gook Park, "Adaptive two-stage extended Kalman filter for a fault-tolerant INS-GPS loosely coupled system," *IEEE Trans. Aerosp. Electron. Syst.*, vol. 45, no. 1, pp. 125–137, Jan. 2009.
- [14] Y. Geng and J. Wang, "Adaptive estimation of multiple fading factors in Kalman filter for navigation applications," *GPS Solutions*, vol. 12, no. 4, pp. 273–279, Sep. 2008.
- [15] K. Myers and B. Tapley, "Adaptive sequential estimation with unknown noise statistics," *IEEE Trans. Autom. Control*, vol. 21, no. 4, pp. 520–523, Aug. 1976.

- [16] B. Jia and M. Xin, "Sparse-grid quadrature  $H_\infty$  filter for discrete time systems with uncertain noise statistics," *IEEE Trans. Aerosp. Electron. Syst.*, vol. 49, no. 3, pp. 1626–1636, 2013.
- [17] B. Jia, M. Xin, and Y. Cheng, "Sparse-grid quadrature nonlinear filtering," *Automatica*, vol. 48, no. 2, pp. 327–341, Feb. 2012.
- [18] Y. Yin, P. Shi, F. Liu, K. Lay Teo, and C.-C. Lim, "Robust filtering for nonlinear nonhomogeneous Markov jump systems by fuzzy approximation approach," *IEEE Trans. Cybern.*, vol. 45, no. 9, pp. 1706–1716, Sep. 2015.
- [19] D. Zhai, X. Liu, C. Xi, and H. Wang, "Adaptive reliable  $H_\infty$  control for a class of T-S fuzzy systems with stochastic actuator failures," *IEEE Access*, vol. 5, pp. 22750–22759, 2017.
- [20] S. J. Julier and J. K. Uhlmann, "Unscented filtering and nonlinear estimation," *Proc. IEEE*, vol. 92, no. 3, pp. 401–422, Mar. 2004.
- [21] S. Julier, J. Uhlmann, and H. F. Durrant-Whyte, "A new method for the nonlinear transformation of means and covariances in filters and estimators," *IEEE Trans. Autom. Control*, vol. 45, no. 3, pp. 477–482, Mar. 2000.
- [22] K. Xiong, H. Y. Zhang, and C. W. Chan, "Performance evaluation of UKF-based nonlinear filtering," *Automatica*, vol. 42, no. 2, pp. 261–270, Feb. 2006.
- [23] L. Chang, B. Hu, A. Li, and F. Qin, "Transformed unscented Kalman filter," *IEEE Trans. Autom. Control*, vol. 58, no. 1, pp. 252–257, Jan. 2013.
- [24] I. Arasaratnam and S. Haykin, "Cubature Kalman filters," *IEEE Trans. Autom. Control*, vol. 54, no. 6, pp. 1254–1269, Jun. 2009.
- [25] Y. Huang and Y. Zhang, "Robust student's t-based stochastic cubature filter for nonlinear systems with heavy-tailed process and measurement noises," *IEEE Access*, vol. 5, pp. 7964–7974, 2017.
- [26] W. Li and Y. Jia, "H-infinity filtering for a class of nonlinear discrete-time systems based on unscented transform," *Signal Process.*, vol. 90, no. 12, pp. 3301–3307, Dec. 2010.
- [27] K. Nishiyama, "A unified view of adaptive algorithms for finite impulse response filters using the  $H_\infty$  framework," *Signal Process.*, vol. 97, pp. 55–63, Apr. 2014.
- [28] Y. Huang, Y. Zhang, N. Li, and J. Chambers, "Robust student's t based nonlinear filter and smoother," *IEEE Trans. Aerosp. Electron. Syst.*, vol. 52, no. 5, pp. 2586–2596, Oct. 2016.
- [29] Y. Huang, Y. Zhang, X. Wang, and L. Zhao, "Gaussian filter for nonlinear systems with correlated noises at the same epoch," *Automatica*, vol. 60, pp. 122–126, Oct. 2015.
- [30] X. Liu, J. Hu, and H. Wang, "Research on integrated navigation method based on adaptive  $H_\infty$  filter," *Chin. J. Sci. Instrum.*, vol. 35, no. 5, pp. 1013–1021, 2014.
- [31] J.-S. Hu and C.-H. Yang, "Second-order extended  $H_\infty$  filter for nonlinear discrete-time systems using quadratic error matrix approximation," *IEEE Trans. Signal Process.*, vol. 59, no. 7, pp. 3110–3119, Jul. 2011.
- [32] Z. Gu, P. Shi, D. Yue, and Z. Ding, "Decentralized adaptive event-triggered  $H_\infty$  filtering for a class of networked nonlinear interconnected systems," *IEEE Trans. Cybern.*, vol. 49, no. 5, pp. 1570–1579, May 2019.
- [33] M. X. Wang and Z. Z. Jia, *Matrix Inequality*. Beijing, China: Science Press, 2006, pp. 160–165.
- [34] D. Goshen-Meskin and I. Y. Bar-Itzhack, "Unified approach to inertial navigation system error modeling," *J. Guid., Control, Dyn.*, vol. 15, no. 3, pp. 648–653, May 1992.
- [35] P. G. Savage, *Strapdown Analytics*, 2nd ed. Maple Plain, MN, USA: Strapdown Associates, 2007.



**WEIWEI LYU** received the M.S. degree from the Nanjing University of Aeronautics and Astronautics, Nanjing, China, in 2015. He is currently pursuing the Ph.D. degree with the School of Instrument Science and Engineering, Southeast University, Nanjing.

He was a Visiting Student with UNSW, Sydney, NSW, Australia, from 2018 to 2019. His research interests include inertial navigation, autonomous underwater vehicle (AUV) integrated navigation, optimal estimation theory, and multisensor information fusion.



**XIANGHONG CHENG** received the Ph.D. degree from the School of Automation, Southeast University, Nanjing, China, in 1998.

She is currently a Professor with the School of Instrument Science and Engineering, Southeast University. Her research interests include inertial navigation and integrated navigation, signal processing, general estimation theory, nonlinear optimal control theory, and nonlinear filtering.



**JINLING WANG** received the Ph.D. degree in Geodesy and GNSS from Curtin University, Perth, WA, Australia, in 1999.

He is currently an Associate Professor with the School of Civil and Environmental Engineering, University of New South Wales (UNSW), Sydney, NSW, Australia. He has published more than 300 articles in journals and conference proceedings, and two commercial software packages. His major research interests are in the areas of navigation and geospatial mapping with multisensors, such as GNSS, INS, pseudolites, LiDAR, and cameras.

• • •